Soil Dynamics and Earthquake Engineering 190 (2025) 109212

Contents lists available at ScienceDirect

Soil Dynamics and Earthquake Engineering

journal homepage: www.elsevier.com/locate/soildyn

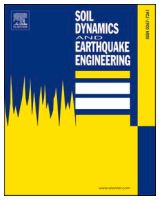

Enhancing soil liquefaction resistance and small-strain dynamic properties using cation-crosslinked biopolymer hydrogel

Dong-Yeup Park [a], Ilhan Chang [b], Minhyeong Lee [c,**], Gye-Chun Cho [a,*]

[a] Department of Civil and Environmental Engineering, Korea Advanced Institute of Science and Technology (KAIST), Daejeon, 34141, Republic of Korea
[b] Department of Civil Systems Engineering, Ajou University, Suwon-si, 16499, Republic of Korea
[c] Disposal Safety Evaluation R&D Division, Korea Atomic Energy Research Institute (KAERI), Daejeon, 34057, Republic of Korea

ARTICLE INFO

Keywords:
Biopolymer-soil stabilization
Liquefaction resistance
Cation-crosslinked xanthan gum
Cyclic simple shear
Dynamic shear modulus
Damping ratio

ABSTRACT

In biopolymer-soil stabilization, biopolymers function in the soil either as viscous fluids or rigid gels. However, the influence of these hydrogel states on soil liquefaction resistance and their underlying mechanisms remain insufficiently understood. This study examines the seismic response of sand treated with biopolymers under small-to-medium strain cyclic loading, with a focus on the efficacy of Cr^{3+}-crosslinked xanthan gum (CrXG) in mitigating liquefaction. Liquefaction resistance and dynamic properties of CrXG-treated soil were compared against thermogelation and non-gelling viscous biopolymer treatments using cyclic direct simple shear and resonant column tests. CrXG treatment at 1 % content improved liquefaction resistance (CRR_{10}) from 0.088 to 0.687 by preventing shear strain accumulation and pore pressure buildup, with enhancing dynamic shear stiffness and delaying stiffness degradation and damping ratio changes to higher strain levels. In contrast, soils treated with non-gelling viscous XG exhibited limited reinforcement under large strain cyclic loading, showing earlier liquefaction and lower CRR_{10} compared than untreated sand, alongside reduced dynamic shear modulus and rapid stiffness degradation. Comparisons across varying earthquake moment magnitudes revealed that CrXG-treated soil achieved liquefaction resistance comparable to other soil stabilization methods and demonstrated greater improvement efficiency than thermogelation biopolymers requiring thermal treatment. These findings highlight the potential of CrXG as a sustainable and practical solution for improving liquefiable soil stability under seismic loading.

1. Introduction

Liquefaction, which is commonly observed during earthquakes in saturated and loose sand deposits, poses a significant threat owing to ground subsidence and structural collapse [1]. This phenomenon occurs under cyclic or vibratory loads in saturated soils, leading to a rapid loss of shear strength as excess pore water pressure accumulates, causing the soil to behave like a liquid [2,3]. Over recent decades, extensive studies have investigated the undrained cyclic loading behavior of sandy soils using through laboratory tests, such as triaxial, torsional, and simple shear tests, to understand the effects of soil composition, structure, and state on liquefaction. Findings reveal that factors like relative density [4,5], fine content [6,7], coefficient of uniformity [8], particle shapes [9,10] and consolidation history critically influence the liquefaction susceptibility and cyclic strength of sandy soils [11–13]. For instance, liquefaction resistance tends to increase with soil density, irrespective of consolidation path, while phase transformation behavior remains similar across various loading conditions [11]. Additionally, aging effects, gravel content, and initial static shear stress are identified as influential in liquefaction behavior, with asymmetrical loading conditions notably alter liquefaction susceptibility and failure mechanisms [12,14]. Further studies underscore the importance of soil fabric [3], void ratio, effective stress, and stress history on liquefaction behavior, prompting the development of reinforcement methods like soil replacement [15], densification [16,17], and chemical solidification [18,19] to mitigate liquefaction in loose sand deposits. However, concerns have emerged over the high energy consumption, costs, and potential environmental issues associated with physical methods and chemical additives, such as cement.

In the context of sustainable soil strengthening, biopolymer-soil

* Corresponding author.
** Co-corresponding author.
E-mail addresses: leemh@kaeri.re.kr (M. Lee), gyechun@kaist.edu (G.-C. Cho).

https://doi.org/10.1016/j.soildyn.2025.109212
Received 2 June 2024; Received in revised form 25 November 2024; Accepted 5 January 2025
Available online 15 January 2025

treatment (BPST) has emerged as an environmentally friendly approach, leveraging exo-cultivated biopolymers derived from living organisms. Notable examples include xanthan gum (XG), corn starch, and guar gum, which have shown effectiveness in enhancing soil properties, such as increasing dry strength, improving erosion resistance, and reducing hydraulic conductivity, even at low dosages across various soil types [20–22]. These improvements stem from mechanisms like particle coating (conglomeration) and pore filling with viscous hydrogels [23–25], along with electrostatic bonding between the polymeric chains and charged clay particles [26,27], making BPST a promising option for mitigating geotechnical hazards. However, BPST faces technical challenges in cohesionless sand. Polysaccharide biopolymer hydrogels, which are typically viscous but non-gelling, have negligible tensile strength in their initial hydrate state, leading to low initial wet strength before dehydration. Their hydrophilic nature also raises concerns about durability under cyclic wetting-drying processes [28,29]. Recent advancements in BPST have introduced gelation methods, such as thermogelation (e.g., agar gum and gellan gum (GG)) and multivalent cation crosslinking (e.g., $Na^{+}/Ca^{2+}/Cr^{3+}$ crosslinked XG), significantly enhancing the initial wet strength in cohesionless soils by forming intergranular connections and pore filling with rigid gel [30–32]. These improvements suggest potential for gelation biopolymer treatment in mitigating shallow-depth liquefaction of cohesionless sands.

A clear understanding of cyclic shear loading required to induce liquefaction and residual pore water pressure in coarse soil is critical for evaluating liquefaction resistance and soil stability under seismic loading [33]. Liquefaction resistance parameters, typically derived from cyclic direct simple shear (CDSS) or cyclic triaxial (CTX) tests, include the cyclic stress ratio (CSR), representing the cyclic shear load relative to vertical or mean stress, and the cyclic resistance ratio (CRR), defined as the CSR at the number of loading cycles (N_L) that induces liquefaction [34,35]. CDSS testing offers a stress field that better replicates the in-situ conditions associated with vertically propagating shear waves, providing valuable insights into CRR [36].

A few of BPST studies on the soil liquefaction have employed CTX tests [37–39]. These tests, particularly under stress- and strain-controlled conditions, have demonstrated that soil stabilization using agar gum, requiring thermogelation at 85°C, effectively reduces excess pore water pressure in sand under cyclic loading [39]. However, the liquefaction resistance of biopolymer-treated soils has not been assessed through CDSS tests, nor has the potential of cation-crosslinked biopolymers, which offer adjustable gelation times and rigidity at ambient temperatures [30], been fully explored. Additionally, limited research has investigated the dynamic shear modulus (G) and damping ratio of biopolymer-treated soils under seismic loading within the small-to-medium strain regime (i.e., $10^{-4} < \gamma < 10^{-2}$), which are essential for ground response analysis.

This study aims to address these research gaps by examining the effect of CrXG biopolymer treatment on the seismic response of sand within the small-to-medium strain regime, particularly focusing on its liquefaction mitigation capabilities. The study compares the liquefaction resistance and dynamic properties of CrXG-treated soil with untreated soils and two other biopolymer-treated soils (thermogelation type and non-gelling viscous type) to evaluate the differences in effectiveness across hydrogel states. Undrained stress-controlled CDSS and resonant column (RC) tests were conducted to analyze cyclic shear responses, excess pore water pressure, CSR, and CRR-N_L relationships, and dynamic properties (G and damping ratio) and their degradation. Based on experimental results, this paper discusses different improvement mechanisms of biopolymers under seismic conditions, evaluates competitiveness of these biopolymer treatments in liquefaction mitigation, and explores potential applications of CrXG treatment as a sustainable strategy for reinforcing shallow soils with high groundwater levels in liquefiable regions.

2. Materials and methods

2.1. Materials

2.1.1. Host soil: jumunjin sand

Jumunjin sand, a coarse-grained soil representative of South Korea and frequently used in liquefaction studies [40–42], was selected for this research. The particle size distribution of this soil is shown in Fig. 1a, with blue lines indicating potentially liquefiable soils and red lines highlighting the range of highest liquefaction susceptibility for sandy soil [43]. Jumunjin sand has a mean particle size (D_{50}) of 0.52 mm and is classified as poorly graded sand (SP), meeting the criteria for liquefiable sands. A microscopic image and basic soil properties of Jumunjin sand, is provided in Fig. 1b.

2.1.2. Biopolymers

This study utilized three polysaccharide biopolymers (XG, CrXG, and GG) categorized into two types: rigid gel and viscous gel. CrXG and GG were classified as rigid gel-type biopolymers, while XG served as a viscous biopolymer.

XG, an anionic polysaccharide, is widely applied across industries due to its versatility. Its carboxylate side chains (–COOH) enhance water affinity, resulting in increased viscosity and swelling upon dissolution [44]. These properties enable XG to form a viscous hydrogel, making it effective as soil thickener [45]. Previous studies have highlighted XG's potential as a soil stabilizer, improving dry compressive and shear strengths [25,46,47], reducing hydraulic conductivity [48], and increasing erosion resistance [49,50]. For this study, analytical-grade XG powder from *Xanthomonas campestris* (Sigma-Aldrich, CAS: 11138-66-2) was used.

CrXG, a crosslinked form of XG with Cr^{3+} cations, was synthesized using chromium nitrate nonahydrate ($Cr(NO_3)_3{\cdot}9H_2O$, 99 %, Daejung Chemical Co.), a highly soluble violet crystal known for its thermodynamic stability and efficient crosslinking [51,52]. Combining Cr^{3+} solutions with XG hydrogel initiates gelation, where Cr^{3+} ions form intermolecular crosslinks with XG's -COO^{-} groups, resulting in a rigid CrXG gel. This transformation enhances geotechnical properties such as wet strength, durability, and shear strength in sand [30,31].

GG, representing thermogelation biopolymers, is produced by *Sphingomonas elodea* and is known for its high molecular weight [53]. GG hydrates as a viscous liquid at room temperature (25 °C), disperses upon heating to above 90°C, and reforms into a rigid hydrogel upon cooling, creating a fibrous structure [54]. Research grade low-acyl GG powder (Sigma-Aldrich, CAS No: 71010-52-1) was used.

2.2. Experimental programs

2.2.1. Sample preparation

The biopolymer-soil mixtures for the CDSS and RC tests were prepared following a multistep process, beginning with hydrogel formation. Fig. 2 illustrates the initial and post-gelation states of XG, CrXG, and GG hydrogels. XG powder was dissolved in distilled water at a concentration of 3.3 % (m_b/m_w = biopolymer mass-to-water mass ratio) using a laboratory mixer. XG hydrogel remains non-gelling and viscous, maintaining a liquid-like consistency unless dehydrated (Fig. 2a). For CrXG hydrogel synthesis, XG hydrogel was blended with an aqueous Cr^{3+} solution prepared with $Cr(NO_3)_3{\bullet}9H_2O$ and NaCl in distilled water, maintaining an m_b/m_w of 3.3 %. The final mass ratio of XG, $Cr(NO_3)_3{\bullet}9H_2O$, and NaCl by mass was set at 10:3:1, based on an optimal mix for wet strength enhancement in sand [31]. Initially, CrXG hydrogel shares a viscous liquid-like state, similar to XG hydrogel alone, but transitions into a rigid gel state due to gradual crosslinking (Fig. 2b). For GG hydrogel preparation, GG powder was dissolved in distilled water heated to 110 °C with a m_b/m_w of 5 % following previous methods [27]. GG forms a viscous liquid after heating but undergoes thermogelation upon cooling to room temperature (25 °C), forming a rigid gel (Fig. 2c)

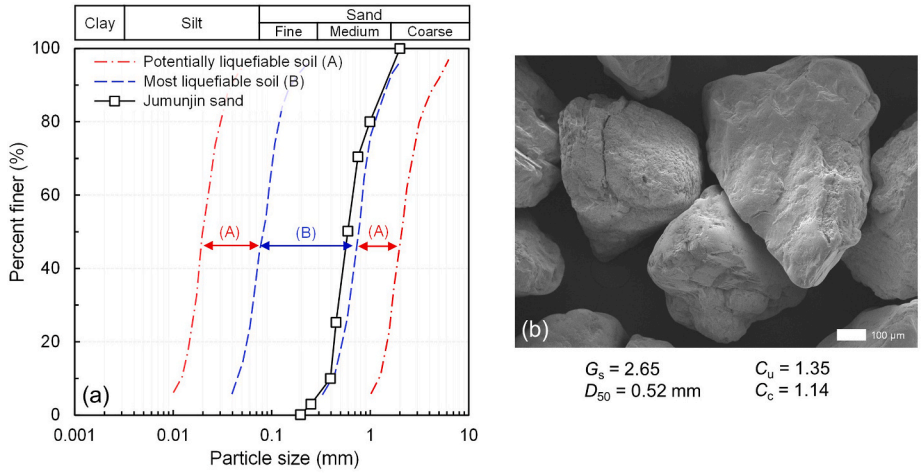

Fig. 1. (a) Particle size distribution, and (b) microscopic image of host soil. Liquefaction susceptibility criteria is referred from Díaz-Rodríguez et al. (2008).

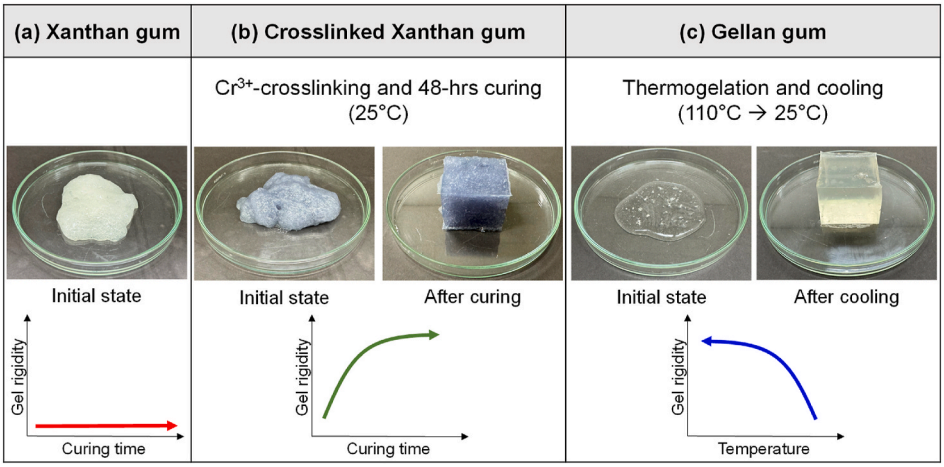

Fig. 2. State of biopolymer hydrogels at initial and post-gelation state.

[27].

After hydrogel preparation, oven-dried sand (heated to 110 °C for 24 h) was thoroughly mixed with each hydrogel to achieve an initial water content (water mass in hydrogel-to-soil mass ratio) of 20 % and biopolymer content (biopolymer mass-to-soil mass ratio) of 1 %, ensuring mixing workability based on previous studies [25,30,54,55]. The mixture was tamped into cylindrical molds for each test, with CDSS specimens measuring 63.5 mm in diameter and 10 mm in height, and RC specimens measuring 50 mm in diameter and 100 mm in height. Control over initial dry densities ensured compactness, with all soil specimens (untreated and biopolymer-treated) within a range of 1480 ± 30 kN/m^3, indicating medium compaction. Untreated and XG-treated specimens were tested immediately after installation. CrXG-treated specimens were pre-cured in molds for 48 h to achieve gelation [30,56], while GG-treated specimens were cooled to room temperature to induce thermogelation [27]. Specimens were sealed to prevent evaporation and maintain water content during the pre-curing.

2.2.2. Cyclic direct simple shear test

Undrained CDSS tests under stress-controlled conditions were conducted using a Shear Trac-II (Geocomp, USA) to investigate the cyclic loading response and liquefaction resistance of untreated and biopolymer-treated specimens (Fig. 3a). Each specimen, measuring 63.5 mm in diameter and 20 mm in height, were positioned in a shear box with a membrane, while Teflon rings providing lateral confinement to ensure zero-horizontal extension. The test was performed under constant volume control with vertical confining pressures (σ_{vc}) of 50 and 100 kPa, where vertical loading was adjusted to maintain a constant sample height, thereby simulating undrained conditions [57]. A two-way sinusoidal shear load was applied at a frequency of 0.1 Hz, with the cyclic stress ratio (CSR) varying from 0.05 to 0.8 depending on the specimen type, reaching a maximum shear strain of 10 % in double amplitude. Excess pore pressure (Δu) was inferred from changes in effective vertical stress (σ'_v) as cyclic shear stress (τ_{cyc}) was applied [57,58]. Liquefaction was defined as occurring when either (1) shear strain exceed 7.5 % double amplitude (DA) shear strain threshold (equivalent to 5 % double amplitude axial strain in a cyclic triaxial tests) or (2) Δu reached the initial σ_{vc} level, indicating a significant reduction in σ'_v [59–61].

2.2.3. Resonant column test

RC tests were conducted using the GTS25 apparatus (GEOTM, Korea) to assess the dynamic properties of biopolymer-treated soil within the small-to-medium γ level ($10^{-4} < \gamma < 10^{-2}$) (Fig. 3b). The specimens size measures 50 mm in diameter and 100 mm in height. Torsional shear loading was applied under fixed-free RC conditions at confining pressures of 100, 200, and 400 kPa. Sinusoidal torsional excitation was delivered to the specimen's top, with torque and rotational responses measured using an accelerometer and proximeter. The driving torque magnitude was progressively increased in successive sweeps within the

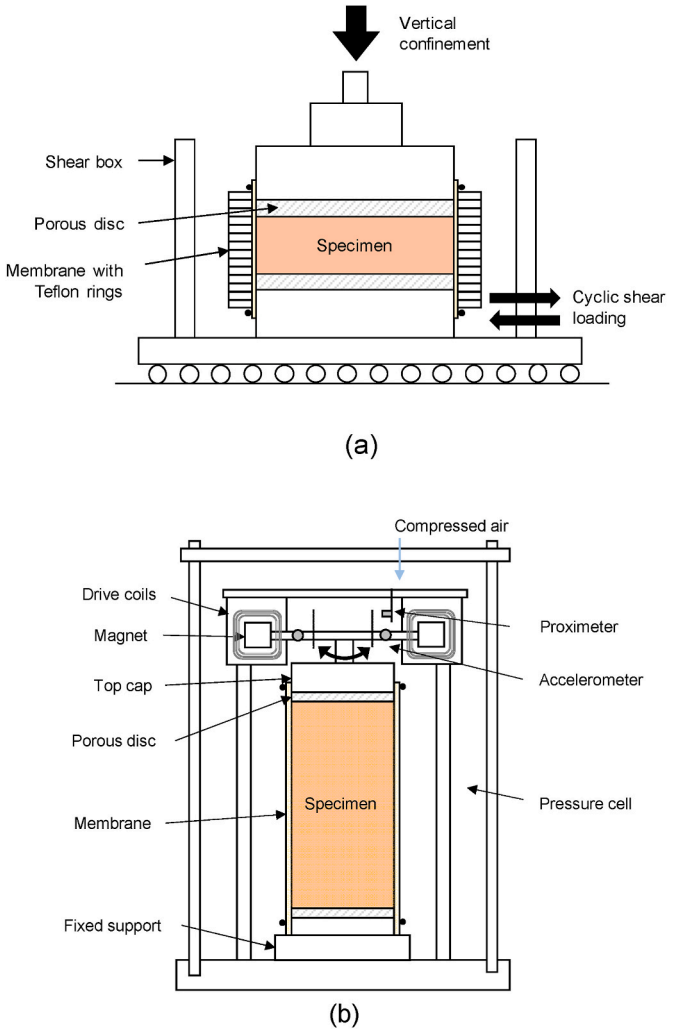

Fig. 3. Experimental testing setups: (a) cyclic direct simple shear test; (b) resonant column test.

target γ range, from 10^{-4} to 10^{-2}. Shear wave velocity and shear modulus (G) were computed based on the moment of inertia ratio between the driving system and the soil specimens, while the damping ratio was derived from the free vibration attenuation curve [62,63].

3. Results and analysis

3.1. Effect of biopolymer treatment on undrained cyclic simple shear responses

The effectiveness of biopolymer treatment in enhancing undrained cyclic resistance was assessed by comparing the cyclic shear responses of untreated and biopolymer-treated specimens under stress-controlled conditions. A summary of the CDSS test results is provided in Table 1.

The representative undrained cyclic shear responses of untreated sand at $\sigma_{vc} = 100$ kPa and CSR = 0.06 are shown in Fig. 4. The cyclic simple shear behavior of untreated sand aligns with trends reported in previous studies on poorly-graded sand subjected to CDSS tests [60,64]. As the number of cycles (N) increased, axial strain accumulated gradually, reaching a peak-to-peak strain of 7.5 % DA after 32 loading cycles, at which point liquefaction was observed (Fig. 4a). The pronounced lateral deformation associated with liquefaction is evident in the $\tau_{cyc} - \gamma$ relationship (Fig. 4b). During cyclic loading, shearing caused a progressive reduction in σ'_v. In CDSS tests, where Δu is determined from $\sigma_{vc} - \sigma'_v$, Δu was observed to increase with N, approaching 100 % around the 32nd cycle, confirming the occurrence of liquefaction.

Table 1
Results of CDSS tests.

Test No.	Sample	σ_{vc} [kPa]	CSR	N_L	CRR-N_L relationship	CRR_{10}
U1	Untreated	50	0.10	19	$0.320 \bullet (N_L)^{-0.333}$	0.148
U2			0.15	17		
U3			0.18	5		
U4			0.20	5		
U5			0.22	3		
U6			0.25	2		
U7		100	0.05	104	$0.162 \bullet (N_L)^{-0.264}$	0.088
U8			0.06	32		
U9			0.07	21		
U10			0.10	8		
U11			0.12	3		
X1	XG 1 %	50	0.08	16	$0.146 \bullet (N_L)^{-0.191}$	0.094
X2			0.09	21		
X3			0.10	5		
X4			0.13	2		
X5			0.15	1		
X6		100	0.06	111	$0.113 \bullet (N_L)^{-0.114}$	0.087
X7			0.07	74		
X8			0.08	14		
X9			0.09	3		
X10			0.10	3		
X11			0.12	1		
G1	GG 1 %	50	0.30	26	$0.459 \bullet (N_L)^{-0.128}$	0.341
G2			0.33	12		
G3			0.35	8		
G4			0.40	4		
G5			0.45	1		
G6		100	0.10	N/A	$0.456 \bullet (N_L)^{-0.149}$	0.324
G7			0.25	59		
G8			0.30	41		
G9			0.33	13		
G10			0.35	6		
G11			0.40	5		
G12			0.41	3		
G13			0.43	1		
C1	CrXG 1 %	50	0.70	60	$0.804 \bullet (N_L)^{-0.029}$	0.752
C2			0.73	51		
C3			0.75	10		
C4			0.77	6		
C5			0.80	1		
C6		100	0.10	N/A	$0.746 \bullet (N_L)^{-0.036}$	0.687
C7			0.63	101		
C8			0.65	44		
C9			0.67	30		
C10			0.68	10		
C11			0.70	5		
C12			0.75	1		

Note: N/A = not available, indicating that the test was manually terminated because of the negligible deformation of the sample even after 100 cycles.

Fig. 5 compares the cyclic simple shear responses of untreated, XG-, GG-, and CrXG-treated soil under $\sigma_{vc} = 100$ kPa and CSR = 0.10, highlighting the impact of biopolymer treatment. The shear strain responses with N revealed significant deformation in the untreated and XG-treated soils within the first 10 cycles. In untreated sand, the peak-to-peak strain reached 7.5 % DA at $N = 8$, while in XG-treated sand, it reached 7.5 % at $N = 3$, satisfying one of the liquefaction criteria (Fig. 5a and b). GG- and CrXG-treated soils also exhibit slight strain at the initiation of loading, attributed to the stretchable properties of the rigid gel [65]. However, unlike XG-treated and untreated soils, where shear strain continues to accumulate, GG-treated (6.1 %) and CrXG-treated soils (2.4 %) maintain strain levels within the 7.5 % DA condition even after 100 cycles (Fig. 5c and d). This reduced deformation in GG- and CrXG-treated soil aligns with the cyclic stress-strain curve (Fig. 5e–h), which demonstrate increasing γ with cycles in untreated and XG-treated soils, whereas the hysteresis loop remained stable within the DA shear strain criteria for GG- and CrXG-treated soil. The cyclic stress path during loading

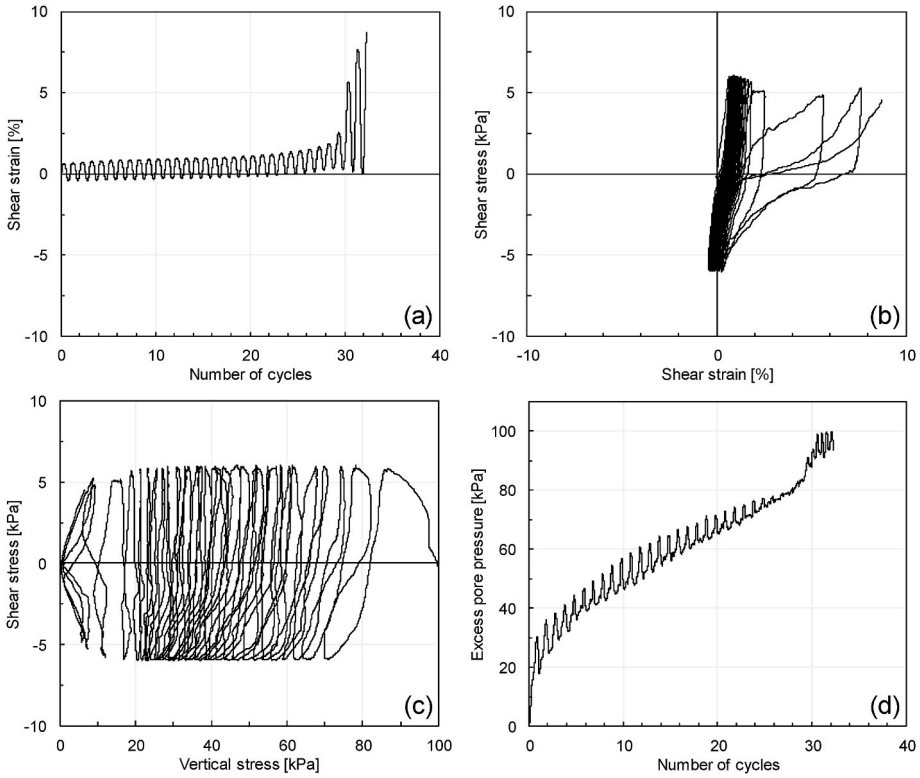

Fig. 4. Undrained cyclic shear responses of untreated sand at $\sigma_{vc} = 100$ kPa and CSR = 0.06. (a) shear strain responses, (b) shear stress-strain curves, (c) cyclic stress paths, and (d) excess pore pressure responses.

(Fig. 5i–l) indicated a gradual reduction in σ_{vc} with increasing cycles, reflecting the development of Δu. According to the liquefaction initiation criteria where the $\Delta u/\sigma_{vc}$ ratio reaches 0.95 [66], liquefaction was confirmed in untreated sand (Fig. 5m). In XG-treated soil (Fig. 5n), Δu increased to 56 kPa at $N = 1$, and the test were terminated with $\Delta u = 79$ kPa at N = 3 without reaching the $\Delta u/\sigma_{vc}$ threshold of 0.95. The smaller Δu observed in XG-treated sand can likely be attributed to its low hydraulic conductivity due to the high water absorption capacity and pore-filling effect of viscous XG hydrogel [67]. In contrast, GG and CrXG-treated soil exhibited moderate Δu increments up to $N = 10$, but did not exceed liquefaction thresholds even at $N = 100$. This suggests that the rigid gel-type biopolymer hydrogels in GG- and CrXG-treated soils prevented liquefaction by delaying pore pressure buildup and minimizing lateral deformation under cyclic loading conditions.

3.2. Cyclic resistance ratio and liquefaction resistance of biopolymer-treated soil

The cyclic resistance ratio (CRR) is commonly used to normalize irregular cyclic loading data into an equivalent number of uniform loading cycles [68]. It is defined as the CSR required to induce liquefaction in a specific number of cycles (N_L) [69]. The relationship between CRR vs. N_L is typically modeled using a power law:

$$CRR = a \bullet N_L^{-b} \quad (1)$$

where the parameters a and b are derived through regression analysis. The parameter a represents the CSR corresponding to a single loading cycle ($N_L = 1$), reflecting the liquefaction resistance of the soil [70,71]. The exponent b indicates the rate of degradation in soil strength or stiffness with increasing cyclic shear strain during loading [72]. In this study, the CRR at $N_L = 10$ (CRR_{10}) was used to compare liquefaction resistances of the soil specimens. This corresponds to an earthquake magnitude of 7, as per the Korean design standard for liquefaction evaluation [73]. The regression parameters for the fitted CSR-N_L relationship and the CRR_{10} values are summarized in Table 1.

Fig. 6 presents the CSR−N_L relationship curves for untreated and biopolymer-treated soils under σ_{vc} of 50 and 100 kPa. The results indicate that higher CSR levels result in liquefaction occurring after fewer loading cycles, whereas lower CSR levels require more loading cycles to induce liquefaction. Across all cases, XG-treated soil, which incorporates a non-gelling viscous biopolymer, shows a lower CSR for liquefaction at a given number of cycles compared to untreated soil. In contrast, GG- and CrXG-treated soils, which utilize rigid gel-forming biopolymers, exhibit significantly higher CSR values at the same N_L, indicating improved resistance to cyclic shear loading. At $\sigma_{vc} = 50$ kPa, the CRR_{10} value for XG-treated soil is 0.094, a 37 % reduction compared to untreated soil ($CRR_{10} = 0.148$). Conversely, GG and CrXG-treated soils show CRR_{10} values of 0.341 and 0.751, representing increases of 130 % and 407 %, respectively. At $\sigma_{vc} = 100$ kPa, the CRR_{10} value for untreated, XG-, GG- and CrXG-treated soils are 0.088, 0.087, 0.324, and 0.687, respectively. These findings demonstrate that biopolymer treatments, particularly those utilizing rigid gel-type biopolymers, significantly enhance liquefaction resistance. In contrast, the XG treatment, which employs a viscous non-gelling biopolymer, provide no substantial improvement in liquefaction resistance relative to untreated soil. This lack of effectiveness is attributed to the absence of structural reinforcement and stiff interparticle bonding in XG-treated sand [47]. The observed trend of increasing CRR values with decreasing confinement pressure aligns with the results of previous studies [43,47,60].

3.3. Effect of biopolymer treatment on dynamic properties of soil

The impact of biopolymer treatment on dynamic shear modulus (G) and damping ratio was evaluated using resonant column tests, with γ increasing across small-to-medium strain ranges. The relationships between G and γ for untreated and biopolymer-treated soils are shown in Fig. 7. At higher confining pressures, the G exhibits greater values. XG-treated sand showed lower G values compared to untreated sand,

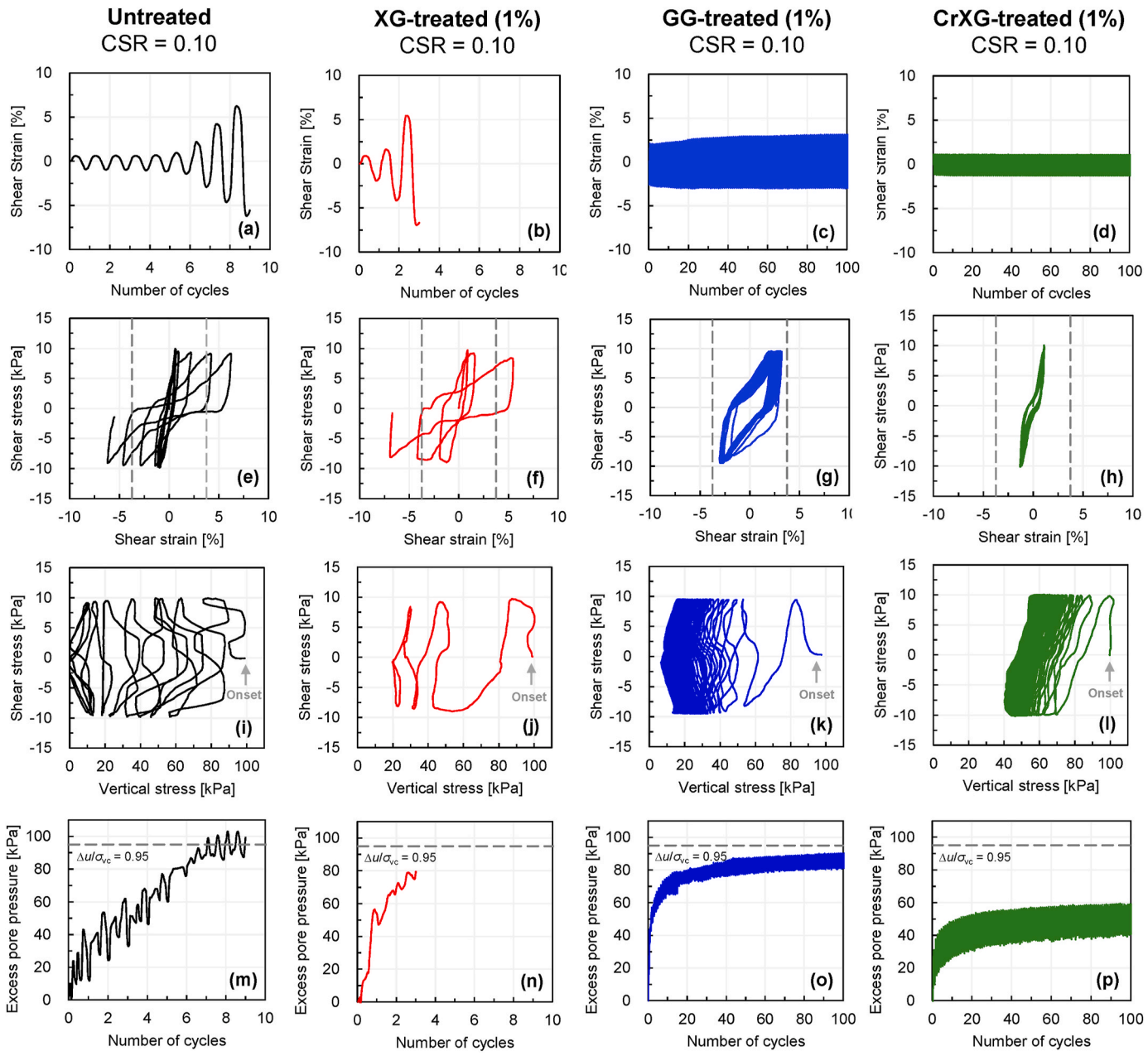

Fig. 5. Cyclic shear responses of untreated and biopolymer-treated soil sheared at CSR = 0.10 under σvc = 100 kPa: (a–d) shear strain responses, (e–h) shear stress-strain curves, (i–l) cyclic stress paths, and (m–p) excess pore pressure responses.

whereas GG- and CrXG-treated sands demonstrated higher G values at same strain level. The contrasting trend observed for XG-treated sand aligns with the results of CDSS tests, highlighting the influence of the viscous hydrogel state. In untreated and XG-treated sands, G decreases significantly with increasing strain, particularly below 10^{-3}. Conversely, GG- and CrXG-treated sands exhibit more gradual reductions in G, indicating their ability to maintain soil structure and stiffness under excitation. This suggests that while XG treatment fails to effectively control deformation, rigid gel-type biopolymers enhance structural stability.

The relationships of G and damping ratio with strain were fitted using the Ramberg-Osgood model (Eq. (2)) [74,75], and Darendeli model (Eq. (3)) [76], respectively:

$$\gamma = \left(\frac{G}{G_{\max}}\right)\gamma + c\left(\frac{G}{G_{\max}}\gamma\right)^{d} \tag{2}$$

$$D = D_{\min} + \frac{k\,(\gamma/\gamma_r)}{1+(\gamma/\gamma_r)} \tag{3}$$

where G is the shear modulus; $G_{\max}$ is the maximum shear modulus; a and b are fitting parameters for the modulus curve; D is the damping ratio, $D_{\min}$ is the minimum damping ratio, and k is a fitting coefficient, and γ_r is the reference shear strain at $G/G_{\max} = 0.5$.

Fig. 8a illustrates $G/G_{\max}$ relationships, with $G_{\max}$ values for each confining pressure summarized in Table 2. GG- and CrXG-treated soils exhibited significantly higher G_{max} values compared to untreated soil, with increases of 74 % and 36 %, respectively, at confining pressure of 100 kPa. In contrast, XG-treated soils showed reductions in G_{max} ranging from 4 % to 29 %, indicating that non-gelling viscous hydrogel reduced the interlocking effect by resisting compaction under confining conditions compared to untreated sand [77,78]. Conversely, the rigid gel-bound structure in GG- and CrXG-treated soils enhanced stiffness,

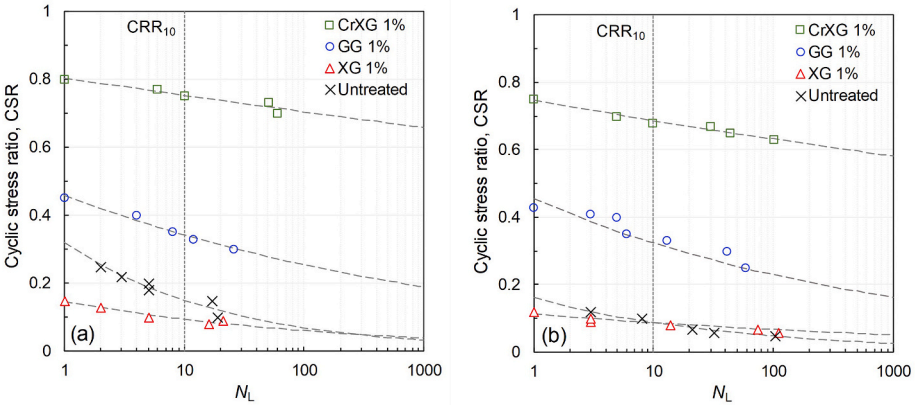

Fig. 6. CSR versus N_L of untreated and biopolymer-treated soils: (a) $\sigma_{vc} = 50$ kPa; (b) $\sigma_{vc} = 100$ kPa.

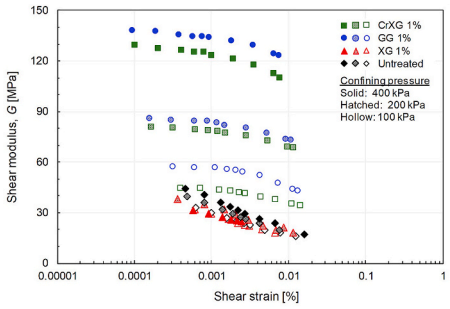

Fig. 7. Variation of dynamic shear modulus of biopolymer-treated soils across shear strains and confining pressures.

even under high confinement.

The G/G_{max} curves revealed a progressive stiffness degradation with increasing γ, which can be characterized by three key strain thresholds [79]. The linear threshold strain (γ_{tl}) occurs at $G/G_{max} = 0.99$, indicating minor fabric changes and no significant pore pressure accumulation during cyclic loading. The volumetric threshold strain (γ_{tv}) is observed at $G/G_{max} = 0.8$, marking the transition between fully recoverable small strain regime and medium strain regime with minor strength degradation. Finally, the degradation threshold strain (γ_{td}) is identified at $G/G_{max} = 0.6$, where rapid shear modulus reduction begins.

Table 3 summarizes the threshold strain values for untreated and biopolymer-treated soils. Untreated and XG-treated soils displayed faster stiffness degradation at strain levels below 10^{-3}. In contrast, CrXG- and GG-treated soils exhibited delayed degradation, initiating between 10^{-3} and 10^{-2}, which is approximately four times larger than

Table 2
Dynamic shear modulus (G_{max}) of untreated- and biopolymer-treated soil.

Confining pressure [kPa]	Dynamic shear modulus, G_{max} [MPa]			
	Untreated	XG 1 %	GG 1 %	CrXG 1 %
100	33.1	31.8	57.7	45.1
200	39.8	38.1	86.4	81.1
400	44.3	31.5	138.4	129.6

that of untreated or XG-treated soils. The similar stiffness degradation patterns in CrXG- and GG-treated soils highlight the role of rigid gels in enhancing dynamic resistance. This delayed degradation can be attributed to increased ductility, the cementation effects of stiff gels, and the hydrogel pore-filling, which effectively prevented excessive pore pressure buildup during loading (Fig. 5o and p).

In the small-strain regime, the damping ratio levels showed minimal variation across soil types but consistently increased with γ for all tested soils (Fig. 8b). However, CrXG- and GG-treated soils demonstrated smaller amplitudes and slower rates of increase in damping ratio

Table 3
Comparison of threshold strain of untreated- and biopolymer-treated soil.

Biopolymer treatment	Untreated	XG 1 %	GG 1 %	CrXG 1 %
Linear threshold strain, γ_{tl} ($G/G_{max} = 0.99$)	1.10×10^{-4}	1.81×10^{-4}	3.11×10^{-4}	3.05×10^{-4}
Volumetric threshold strain, γ_{tv} ($G/G_{max} = 0.80$)	1.59×10^{-3}	2.00×10^{-3}	1.63×10^{-2}	1.22×10^{-2}
Degradation threshold strain, γ_{td} ($G/G_{max} = 0.60$)	4.49×10^{-3}	5.21×10^{-3}	6.80×10^{-2}	4.69×10^{-2}

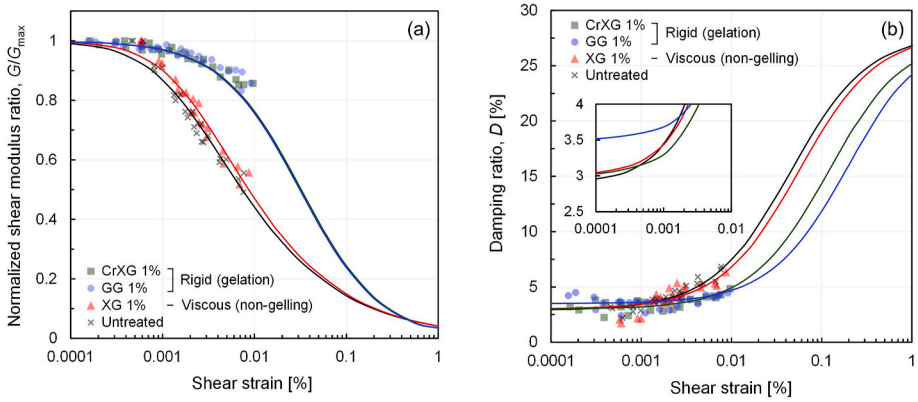

Fig. 8. (a) G/G_{max} - γ curve, and (b) damping ratio - γ curve for untreated and biopolymer-treated soil.

compared to untreated and XG-treated soils. This behavior indicates less energy dissipation in CrXG- and GG-treated soils, coupled with their enhanced ability to maintain structural integrity under large displacements.

4. Discussions

4.1. Role of different biopolymer hydrogels in sand under seismic loading

When seismic loads are applied to saturated, loosely packed soils, shear strength is rapidly lost due to excess pore water pressure buildup, resulting in liquefaction. Experimental results highlight distinct influence of biopolymer hydrogels, depending on their state, on soil resistance to shear deformation under seismic loading. This section discusses the role of biopolymer hydrogel in the soil matrix during seismic loading based on their state. Fig. 9 presents a schematic figure illustrating the effects of biopolymer hydrogels in sand: non-gelling viscous type and gelation type, supported by environmental scanning electron microscope (ESEM, Quattro S, Thermo Fisher Scientific Inc.) images of XG- and CrXG-treated sand specimens captured under humid conditions.

The behavior of sand under cyclic loading is influenced by the interaction between the soil skeleton and the pore fluid. Energy dissipation occurs through skeleton damping from particle rearrangement at grain contacts and viscous damping from pore fluid-solid particle interactions [80]. The viscous XG hydrogel aids in energy dissipation through internal friction and viscous drag as seismic waves pass through, functioning as a viscous damper and slightly enhancing damping ratios at small-strain levels [81,82]. Additionally, the high yield stress and water-absorptive properties of XG hydrogel restrict water movement through pore-filling, alleviating pore pressure buildup by restricting water movement through pore-filling. Nevertheless, its minimal tensile strength in hydrated state and shear-thinning behavior limit its structural reinforcement within soil matrix [83]. These properties create a lubricating effect, reducing interparticle friction and shear resistance under large-strain cyclic loading. Consequently, XG-treated sand is more prone to deformation under cyclic loading, as evidenced by its decreased CRR_{10} value compared to untreated sand under $\sigma_v = 50$ kPa.

In contrast, rigid hydrogels achieved through cation crosslinking or thermogelation form mechanical bonds between sand particles, as shown in ESEM images. These hydrogels significantly enhance CRR_{10} and G_{max}. This reinforcement is attributed to the substantial rigidity and tensile strength (50–500 kPa) of CrXG and GG hydrogels [83], creating a cementation effect that strengthens cohesion and prevents particle rearrangement while maintaining effective stress [30,84]. The rigid structure of these hydrogels also delays shear stiffness degradation within the elastic strain range, as seismic energy dissipation at rigid hydrogel-sand interfaces is lower compared to viscous hydrogel-treated soils.

These contrasting reinforcement effects of biopolymer hydrogels align with findings from unconfined compressive strength (UCS) tests [30] (Fig. 10). Under unconfined loading, XG-treated soil exhibits low strength (~10 kPa), while GG and CrXG-treated soils (48-h cured) demonstrate strengths of 123 and 265 kPa, respectively, paralleling the CRR_{10} improvement trend. The tensile strength deficiency of XG hydrogel can potentially be addressed through Cr^{3+} crosslinking, enhancing its applicability for seismic soil stabilization, including liquefaction mitigation at shallow depths.

On the other hand, gelation-type biopolymer-treated sands exhibit a marked delay in shear stiffness degradation within the elastic strain range. This delay minimizes deformations during cyclic loading, effectively reducing settlement risks. However, the reduced energy dissipation associated with rigid hydrogels may lead to amplified ground accelerations and higher dynamic forces at the surface, as the treated soil transmits seismic energy more efficiently without sufficient damping. This trade-off between increased stiffness and potential acceleration amplification may induce dynamic responses in surface structures, potentially causing damages if seismic energy concentrates at specific frequencies [85]. Therefore, careful management in seismic stabilization designs is necessary, and a deeper understanding of soil-structure interactions in biopolymer-treated soil layers is essential for assessing the implications of rigid gel-type biopolymers in enhancing seismic resistance.

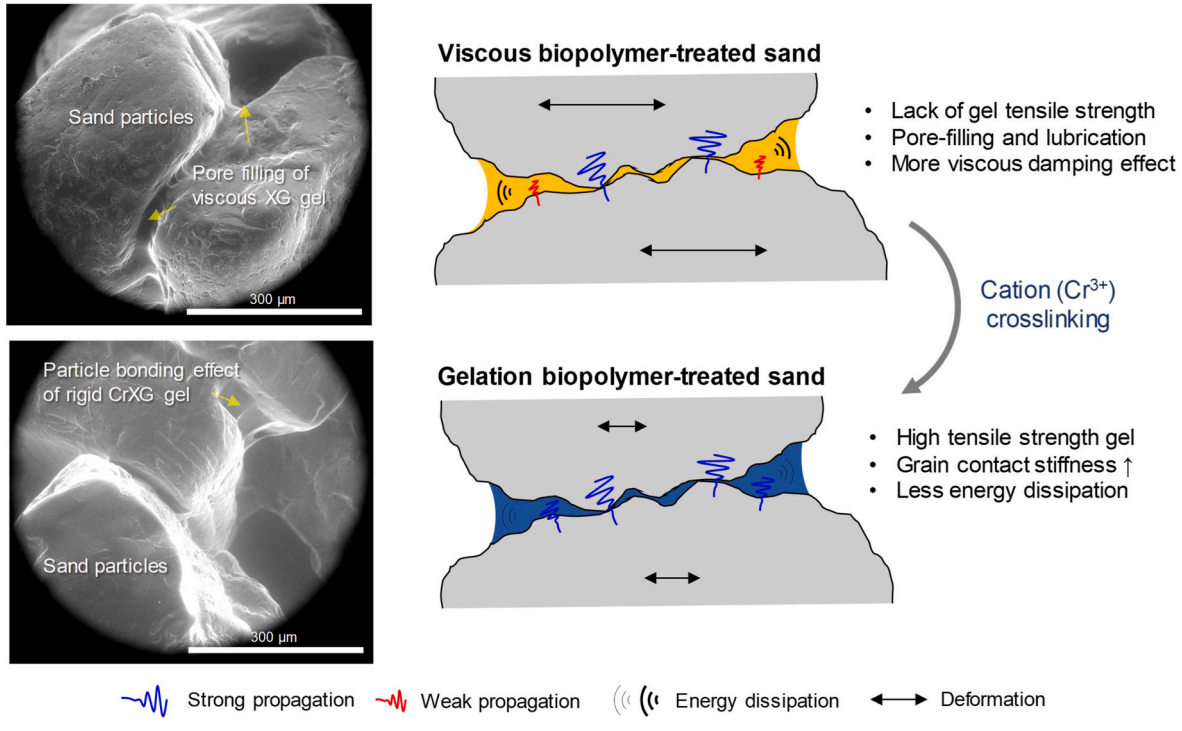

Fig. 9. Conceptual schematic and ESEM images of biopolymer hydrogel effects in sand depending on hydrogel state under seismic loading.

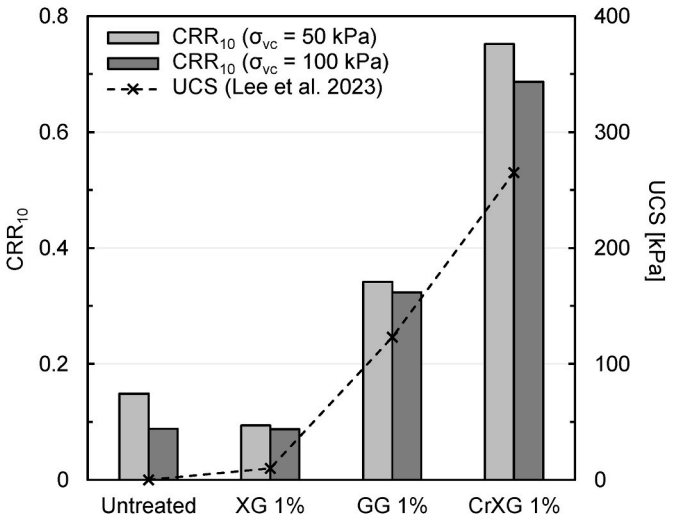

Fig. 10. Comparison of CRR_{10} and UCS of biopolymer-treated soil.

4.2. Comparison of liquefaction resistance improvement efficiency with other soil stabilizers

Fig. 11 presents a comparative analysis of CRR_{10} values at $\sigma_{vc} = 100$ kPa, highlighting the liquefaction resistance improvement efficiency of CrXG biopolymer treatment alongside conventional soil stabilization using agar gum [39], microbially-induced calcite precipitation (MICP) [86], silica grout [43], cement paste [71], and silica sol [87]. The hatched region in figure denotes the CRR_{10} value of each untreated sandy soil. Results indicate that CrXG treatment efficiently enhances liquefaction resistance, achieving levels comparable to microbial and chemical grout cementation methods. Notably, CrXG demonstrated competitive improvement efficiency compared to cement paste, underscoring its potential as a sustainable alternative that addresses concerns related to carbon emissions. Additionally, CrXG treatment achieved higher improvement efficiency compared to GG and agar gum treatments, which required high-temperature heating. The advantages of the CrXG treatment, including its adjustable gelation time and rigidity without thermal processing [31], underscore its low energy requirements and high feasibility for field applications.

To further quantify the improvement in liquefaction resistance, the improvement factor (I_f) was calculated, defined as the ratio of CRR for treated specimens to that of untreated specimens. The formula, as outlined in Eq. (4), provides a standardized metric for comparing the enhancement across different soil stabilization techniques and cyclic loading conditions corresponding to earthquake moment magnitudes (M_w) [88]:

$$I_f = \frac{CRR_{T=N_L}}{CRR_{UT=N_L}} \tag{4}$$

Where $CRR_{T=NL}$ represents the cyclic resistance ratio of biopolymer-treated sand, $CRR_{UT=NL}$ corresponds to untreated sand. Fig. 12 presents the relationship between I_f and M_w for untreated and biopolymer-treated soil in comparison with MICP-treated soil at $\sigma_{vc} = 100$ kPa [86]. For earthquakes with M_w values of 6.0, 7.0, and 7.5—corresponding to 5, 10, and 15 loading cycles, respectively— the XG treatment showed minimal changes in I_f change, reflecting the limited impact of viscous XG hydrogel on seismic performance. In contrast, CrXG-treated soil demonstrated significant increases in I_f with M_w, reaching values between 6.7 and 10.3, far exceeding the range of 1.3–1.4 observed for MICP treatment. This notable improvement highlights CrXG treatment as a competitive liquefaction prevention technique. Its superior I_f values and sustainable attributes position it as a practical alternative for enhancing soil stability in seismic zones, offering substantial promise for widespread application.

4.3. Implications and limitations

The findings from this study suggest that CrXG biopolymer treatment enhances the liquefaction resistance of soils, particularly in shallow soils with high groundwater levels. For field applications in shallow layer,

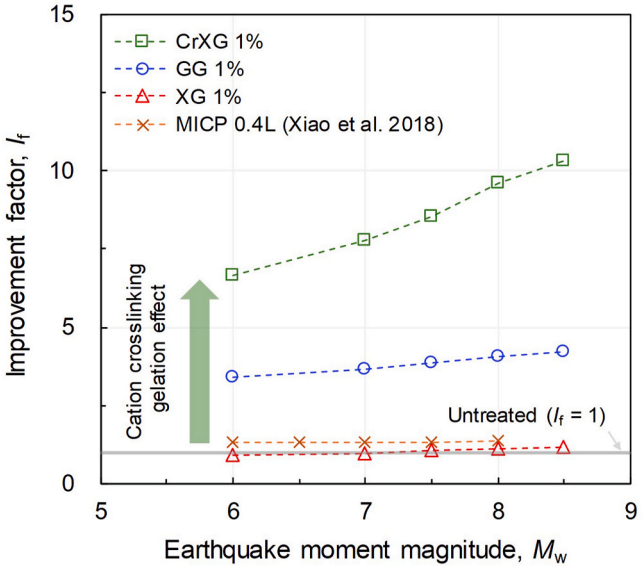

Fig. 12. Improvement factor of liquefaction resistance against moment magnitude of biopolymer-treated and MICP-treated soil.

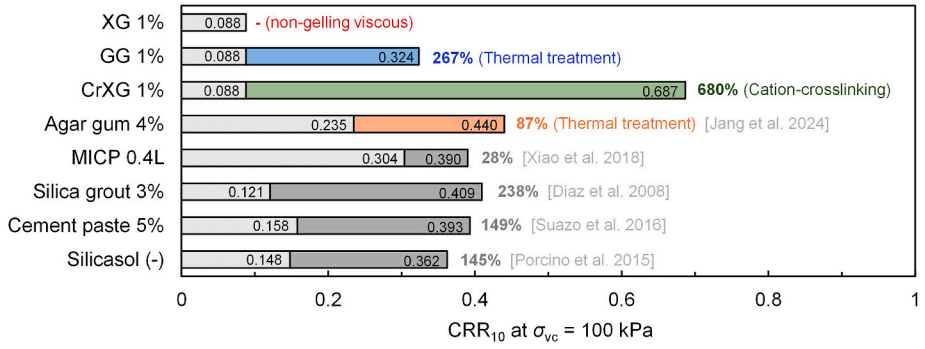

Fig. 11. Comparison of CRR_{10} at $\sigma_{vc} = 100$ kPa and liquefaction resistance improvement efficiency for bio-based and conventional soil stabilizers. The hatched area denotes the CRR_{10} value associated with each untreated sandy soil.

permeation grouting method emerges as a feasible technique. However, the reinforcing performance is heavily dependent on the gel saturation level within soil pore spaces, which is influenced by injection pressure, soil properties, and hydrogel's rheological properties [89–91]. Ensuring uniform distribution of the hydrogel within the treated layer is essential for sustained effectiveness, highlighting the need for further studies to address these practical implementation factors using injection methods.

The biopolymer-treated layer is likely to experience cyclic groundwater fluctuations, altering the moisture state and potentially affecting the strength durability of CrXG-treated soil. While CrXG-treated sand retains wet strength in immersed conditions, moisture loss can reduce particle bonding capacity as the rigid hydrogel transitions into a CrXG film, potentially causing shrinkage-induced fissures [86]. Future studies should investigate the effects of weathering processes on seismic resistance to comprehensively evaluate long-term durability and performance.

It should also be noted that this study assessed liquefaction behavior in CDSS tests using indirect pore water pressure measurements. To gain deeper insights into the pore water pressure generation characteristics in liquefiable soils, further investigations incorporating cyclic triaxial tests with direct PWP measurements would enhance the robustness and applicability of the findings.

5. Conclusion

This study evaluated the feasibility of CrXG biopolymer treatment for liquefaction mitigation by examining its effects on the cyclic shear loading response and dynamic properties of sand within the small-to-medium strain regime. The liquefaction resistance, dynamic shear modulus, and damping ratio of CrXG-treated soils were assessed through cyclic direct simple shear (CDSS) and resonant column (RC) tests and compared with non-gelling viscous XG and thermogelation GG treatments to elucidate their distinct reinforcing mechanisms. The key findings are summarized as follows:

1. The CDSS tests demonstrated that CrXG-treated soil significantly enhances liquefaction resistance by reducing shear strain accumulation and pore pressure development, outperforming untreated and XG-treated soils. Under identical vertical confinement and CSR conditions, XG-treated soils exhibited rapid deformation and lower CRR_{10} compared to untreated sand. While XG hydrogel restricted water movement through pore-filling, its minimal tensile strength in the hydrated state and shear-thinning behavior limited its structural reinforcement within the soil matrix, leading to early liquefaction. Conversely, rigid-gel biopolymer-treated soils, such as CrXG and GG, exhibited stable structures with substantially higher CRR_{10} values. This improvement is attributed to the mechanical bonds formed by the rigid hydrogels, which enhance interparticle cohesion and prevent particle rearrangement while maintaining effective stress.
2. RC test results highlighted the dependence of dynamic shear modulus and damping ratio on the biopolymer hydrogel state. XG-treated soils showed reduced maximum dynamic shear modulus and rapid stiffness degradation due to the limited reinforcing capacity of viscous hydrogels. In contrast, GG- and CrXG-treated soils exhibited significant improvements in dynamic shear stiffness across all confining pressures due to their rigid gel-bound structures. Rigid gels also delayed stiffness degradation to higher strain levels, indicating superior resistance to dynamic loading but reduced seismic energy dissipation. This rigidity minimizes deformations during cyclic loading, effectively mitigating settlement risks. However, it may also amplify ground accelerations and dynamic forces at the surface, necessitating further studies on seismic soil-structure interactions in biopolymer-treated layer.
3. Comparisons of CRR_{10} values at $\sigma_{vc} = 100$ kPa revealed that CrXG treatment achieved liquefaction resistance levels comparable to microbial and chemical grout cementation methods while demonstrating higher improvement efficiency than thermogelation biopolymers that require thermal treatment. Analysis of the improvement factor (I_f) across different earthquake moment magnitudes (M_w) showed minimal changes for XG-treated soils, reflecting the limited impact of viscous hydrogels on seismic performance. In contrast, CrXG-treated soils exhibited significant increases in I_f with M_w, reaching values between 6 and 10. These results highlight CrXG's superior performance and its potential as a sustainable and practical solution for enhancing soil stability in seismic zones.
4. For field applications in shallow layers, permeation grouting emerges as a feasible technique for implementing CrXG treatment for liquefaction mitigation. However, achieving uniform hydrogel distribution within the treated layer requires further investigation into practical parameters, including injection pressure, soil properties, and hydrogel rheology. Additionally, biopolymer-treated layers are likely to experience cyclic groundwater fluctuations, altering their moisture state and potentially affecting the durability of CrXG-treated soils. Future studies should focus on understanding the effects of weathering processes on seismic resistance to comprehensively evaluate long-term performance and durability.

CRediT authorship contribution statement

Dong-Yeup Park: Methodology, Investigation, Formal analysis, Writing - Original draft. **Ilhan Chang:** Conceptualization, Methodology, Validation, Supervision. **Minhyeong Lee:** Conceptualization, Formal analysis, Visualization, Validation, Supervision, Writing - Review & Editing. **Gye-Chun Cho:** Supervision, Validation, Project administration, Funding acquisition.

Declaration of competing interest

The authors declare that they have no known competing financial interests or personal relationships that could have appeared to influence the work reported in this paper.

Acknowledgments

This research was supported by the Ministry of Oceans and Fisheries (MOF) of the Korean Government [No. 20220364] and National Research Foundation of Korea (NRF) funded by the Korean government (MSIT) [No. 2023R1A2C300559611]. Authors appreciate the Korea Institute of Civil Engineering and Building Technology (KICT) by providing technical support regarding to the cyclic simple shear apparatus.

Data availability

Data will be made available on request.

References

[1] Zhu JQ, Wu SP, Zhong JJ, Wang DM. Investigation of asphalt mixture containing demolition waste obtained from earthquake-damaged buildings. Construct Build Mater 2012;29:466–75. https://doi.org/10.1016/j.conbuildmat.2011.09.023.
[2] Dobry R, Abdoun T. Recent findings on liquefaction triggering in clean and silty sands during earthquakes. J Geotech Geoenviron Eng 2017;143:04017077. https://doi.org/10.1061/(ASCE)GT.1943-5606.0001778.
[3] Fardad Amini P, Wang G. Integrated effects of inherent and induced anisotropy on reliquefaction resistance of Toyoura sand with different strain histories. Geotechnique 2023:1–15.
[4] Rouholamin M, Bhattacharya S, Orense RP. Effect of initial relative density on the post-liquefaction behaviour of sand. Soil Dynam Earthq Eng 2017;97:25–36. https://doi.org/10.1016/j.soildyn.2017.02.007.
[5] De Alba PA, Chan CK, Seed HB. Sand liquefaction in large-scale simple shear tests. J Geotech Eng Div 1976;102:909–27. https://doi.org/10.1061/AJGEB6.0000322.
[6] Porcino DD, Diano V. The influence of non-plastic fines on pore water pressure generation and undrained shear strength of sand-silt mixtures. Soil Dynam Earthq Eng 2017;101:311–21. https://doi.org/10.1016/j.soildyn.2017.07.015.

[7] Derakhshandi M, Rathje EM, Hazirbaba K, Mirhosseini SM. The effect of plastic fines on the pore pressure generation characteristics of saturated sands. Soil Dynam Earthq Eng 2008;28:376–86. https://doi.org/10.1016/j.soildyn.2007.07.002.

[8] Monkul MM, Etminan E, Senol A. Influence of coefficient of uniformity and base sand gradation on static liquefaction of loose sands with silt. Soil Dynam Earthq Eng 2016;89:185–97. https://doi.org/10.1016/j.soildyn.2016.08.001.

[9] Rui SJ, Guo Z, Si TL, Li YJ. Effect of particle shape on the liquefaction resistance of calcareous sands. Soil Dynam Earthq Eng 2020;137:106302. https://doi.org/10.1016/j.soildyn.2020.106302.

[10] Ashmawy AK, Hoang VV, Sukumaran B. Evaluating the influence of particle shape on liquefaction behavior using discrete element modeling. In: ISOPE international ocean and polar engineering conference. ISOPE; 2003. ISOPE-I-03-161.

[11] Georgiannou V, Konstadinou M. Effects of density on cyclic behaviour of anisotropically consolidated Ottawa sand under undrained torsional loading. Geotechnique 2014;64:287–302.

[12] Kokusho T. Major advances in liquefaction research by laboratory tests compared with in situ behavior. Soil Dynam Earthq Eng 2016;91:3–22.

[13] Pan K, Yang Z. Effects of initial static shear on cyclic resistance and pore pressure generation of saturated sand. Acta Geotechnica 2018;13:473–87.

[14] Pan K, Xu T, Liao D, Yang Z. Failure mechanisms of sand under asymmetrical cyclic loading conditions: experimental observation and constitutive modelling. Geotechnique 2022;72:162–75.

[15] Sharma M, Satyam N, Reddy KR. Strength enhancement and lead immobilization of sand using consortia of bacteria and blue-green algae. J. Hazardous Toxic Radioact Waste 2020;24:04020049. https://doi.org/10.1061/(ASCE)HZ.2153-5515.0000548.

[16] Olarte JC, Dashti S, Liel AB, Paramasivam B. Effects of drainage control on densification as a liquefaction mitigation technique. Soil Dynam Earthq Eng 2018;110:212–31. https://doi.org/10.1016/j.soildyn.2018.03.018.

[17] Shahir H, Pak A, Ayoubi P. A performance-based approach for design of ground densification to mitigate liquefaction. Soil Dynam Earthq Eng 2016;90:381–94. https://doi.org/10.1016/j.soildyn.2016.09.014.

[18] Bao XH, Jin ZY, Cui HZ, Chen XS, Xie XY. Soil liquefaction mitigation in geotechnical engineering: an overview of recently developed methods. Soil Dynam Earthq Eng 2019;120:273–91. https://doi.org/10.1016/j.soildyn.2019.01.020.

[19] Huang Y, Wen ZQ. Recent developments of soil improvement methods for seismic liquefaction mitigation. Nat Hazards 2015;76:1927–38. https://doi.org/10.1007/s11069-014-1558-9.

[20] Bouazza A, Gates WP, Ranjith PG. Hydraulic conductivity of biopolymer-treated silty sand. Geotechnique 2009;59:71–2. https://doi.org/10.1680/geot.2007.00137.

[21] Cabalar AF, Awraheem MH, Khalaf MM. Geotechnical properties of a low-plasticity clay with biopolymer. J Mater Civ Eng 2018;30:04018170. https://doi.org/10.1061/(ASCE)MT.1943-5533.0002380.

[22] Chang I, Lee M, Tran ATP, Lee S, Kwon YM, Im J, Cho GC. Review on biopolymer-based soil treatment (BPST) technology in geotechnical engineering practices. Transport. Geotech. 2020;24:100385. https://doi.org/10.1016/j.trgeo.2020.100385.

[23] Kwon YM, Moon JH, Cho GC, Kim YU, Chang I. Xanthan gum biopolymer-based soil treatment as a construction material to mitigate internal erosion of earthen embankment: a field-scale. Construct Build Mater 2023;389:131716. https://doi.org/10.1016/j.conbuildmat.2023.131716.

[24] Kwon YM, Kangb SJ, Choc GC, Chang I. Effect of microbial biopolymers on the sedimentation behavior of kaolinite. Geomech Eng 2023;33:121–31. https://doi.org/10.12989/gae.2023.33.2.121.

[25] Chang I, Im J, Prasidhi AK, Cho GC. Effects of Xanthan gum biopolymer on soil strengthening. Construct Build Mater 2015;74:65–72. https://doi.org/10.1016/j.conbuildmat.2014.10.026.

[26] Kwon YM, Chang IL, Cho GC. Consolidation and swelling behavior of kaolinite clay containing xanthan gum biopolymer. Acta Geotechnica 2023;18:3555–71. https://doi.org/10.1007/s11440-023-01794-8.

[27] Chang I, Cho GC. Shear strength behavior and parameters of microbial gellan gum-treated soils: from sand to clay. Acta Geotechnica 2019;14:361–75. https://doi.org/10.1007/s11440-018-0641-x.

[28] Soldo A, Miletic M, Auad ML. Biopolymers as a sustainable solution for the enhancement of soil mechanical properties. Sci Rep 2020;10:267. https://doi.org/10.1038/s41598-019-57135-x.

[29] Lee M, Kwon YM, Park DY, Chang I, Cho GC. Durability and strength degradation of xanthan gum based biopolymer treated soil subjected to severe weathering cycles. Sci Rep 2022;12:19453. https://doi.org/10.1038/s41598-022-23823-4.

[30] Lee M, Chang I, Park DY, Cho GC. Strengthening and permeability control in sand using Cr3+-crosslinked xanthan gum biopolymer treatment. Transport. Geotech. 2023;43:101122. https://doi.org/10.1016/j.trgeo.2023.101122.

[31] Lee M, Chang IL, Cho GC. Advanced biopolymer-based soil strengthening binder with trivalent chromium-xanthan gum crosslinking for wet strength and durability enhancement. J Mater Civ Eng 2023;35:04023360. https://doi.org/10.1061/JMCEE7.MTENG-16123.

[32] Lee M, Chang I, Kang SJ, Lee DH, Cho GC. Alkaline induced-cation crosslinking biopolymer soil treatment and field implementation for slope surface protection. Geomech Eng 2023;33:29–40. https://doi.org/10.12989/gae.2023.33.1.029.

[33] Finn W, Ledbetter R, Marcuson III W. The evolution of geotechnical earthquake engineering practice in North America: 1954-1994. 1995.

[34] Ishihara K. Soil behaviour in earthquake geotechnics. Oxford University Press; 1996. https://doi.org/10.1093/oso/9780198562245.001.0001.

[35] Towhata I. History of geotechnical earthquake engineering in Japan. In: The 14th world conference on earthquake engineering. Beijing, China: October; 2008.

[36] Kramer SL. Geotechnical earthquake engineering. Pearson Education India; 1996.

[37] Smitha S, Rangaswamy K. Effect of biopolymer treatment on pore pressure response and dynamic properties of silty sand. J Mater Civ Eng 2020;32:04020217. Artn0402021710.1061/(Asce)Mt.1943-5533.0003285.

[38] Smitha S, Rangaswamy K. Effect of different parameters on cyclic triaxial response of biopolymer treated soil. Euro J Environ Civil Eng 2022;26:7645–63. https://doi.org/10.1080/19648189.2021.2004451.

[39] Jang C, Yang B, Hong W-T, Ahn J, Jung J. Soil improvement using agar gum polymer for seismic liquefaction mitigation. Soil Dynam Earthq Eng 2024;177:108405. https://doi.org/10.1016/j.soildyn.2023.108405.

[40] Kim Y-S, Ko H-W, Kim J-H, Lee J-G. Dynamic deformation characteristics of Joomunjin standard sand using cyclic triaxial test. J Kor Geotech Soc 2012;28:53–64. https://doi.org/10.7843/kgs.2012.28.12.53.

[41] Seo H, Kim D. Analysis of the characteristics of liquidization behavior of sand ground in Korea using repeated triaxial compression test. J Eng Geol 2021;31:493–506. https://doi.org/10.9720/kseg.2021.4.493.

[42] Kim J, Kwak T-Y, Han J-T, Hwang B-Y, Kim K-S. Evaluation of dynamic ground properties of Pohang area based on in-situ and laboratory test. J Kor Geotech Soc 2020;36:5–20. https://doi.org/10.7843/kgs.2020.36.9.5.

[43] Díaz-Rodríguez J, Antonio-Izarraras V, Bandini P, López-Molina J. Cyclic strength of a natural liquefiable sand stabilized with colloidal silica grout. Can Geotech J 2008;45:1345–55.

[44] Hatakeyama H, Hatakeyama T. Interaction between water and hydrophilic polymers. Thermochim Acta 1998;308:3–22. https://doi.org/10.1016/S0040-6031(97)00325-0.

[45] Melo Cd, Garcia PS, Grossmann MVE, Yamashita F, Dall'Antônia LH, Mali S. Properties of extruded xanthan-starch-clay nanocomposite films. Braz Arch Biol Technol 2011;54:1223–333. https://doi.org/10.1590/S1516-89132011000600019.

[46] Soldo A, Miletic M. Study on shear strength of xanthan gum-amended soil. Sustainability 2019;11:6142. https://doi.org/10.3390/su11216142.

[47] Lee S, Chang I, Chung MK, Kim Y, Kee J. Geotechnical shear behavior of Xanthan Gum biopolymer treated sand from direct shear testing. Geomech Eng 2017;12:831–47. https://doi.org/10.12989/gae.2017.12.5.831.

[48] Tran TPA, Im J, Cho G-C, Chang I. Soil—water characteristics of xanthan gum biopolymer containing soils. In: Proceedings of the 19th international conference on soil mechanics and geotechnical engineering, Seoul; 2017. p. 1091–4.

[49] Chang I, Prasidhi AK, Im J, Shin HD, Cho GC. Soil treatment using microbial biopolymers for anti-desertification purposes. Geoderma 2015;253:39–47. https://doi.org/10.1016/j.geoderma.2015.04.006.

[50] Singh SP, Das R. Geo-engineering properties of expansive soil treated with xanthan gum biopolymer, Geomechanics and Geoengineering-an. Int J 2020;15:107–22. https://doi.org/10.1080/17486025.2019.1632495.

[51] Baruthio F. Toxic effects of chromium and its compounds. Biol Trace Elem Res 1992;32:145–53. https://doi.org/10.1007/BF02784599.

[52] Biamino S, Badini C. Combustion synthesis of lanthanum chromite starting from water solutions: investigation of process mechanism by DTA-TGA-MS. J Eur Ceram Soc 2004;24:3021–34. https://doi.org/10.1016/j.jeurceramsoc.2003.10.005.

[53] Bajaj IB, Survase SA, Saudagar PS, Singhal RS. Gellan gum: fermentative production, downstream processing and applications. Food Technol Biotechnol 2007;45:341–54.

[54] Im J, Tran ATP, Chang I, Cho GC. Dynamic properties of gel-type biopolymer-treated sands evaluated by Resonant Column (RC) Tests. Geomech Eng 2017;12:815–30. https://doi.org/10.12989/gae.2017.12.5.815.

[55] Chang I, Im J, Lee SW, Cho GC. Strength durability of gellan gum biopolymer-treated Korean sand with cyclic wetting and drying. Construct Build Mater 2017;143:210–21. https://doi.org/10.1016/j.conbuildmat.2017.02.061.

[56] Bang J-U, Lee M, Park D-Y, Chang I, Cho G-C. Effects of soil composition and curing conditions on the strength and durability of Cr3+-crosslinked biopolymer-soil composites. Construct Build Mater 2024;449:138440.

[57] Finn W, Vaid Y. Liquefaction potential from drained constant volume cyclic simple shear tests. In: Proceedings of the 6th world conference on earthquake engineering; 1977. p. 10–4. New Delhi, India.

[58] Andersen KH. Bearing capacity under cyclic loading - offshore, along the coast, and on land. The 21st Bjerrum Lecture presented in Oslo, 23 November 2007. Can Geotech J 2009;46:513–35. https://doi.org/10.1139/T09-003.

[59] Da Fonseca AV, Soares M, Fourie A. Cyclic DSS tests for the evaluation of stress densification effects in liquefaction assessment. Soil Dynam Earthq Eng 2015;75:98–111.

[60] Park SS, Nong ZZ, Lee DE. Effect of vertical effective and initial static shear stresses on the liquefaction resistance of sands in cyclic direct simple shear tests. Soils Found 2020;60:1588–607. https://doi.org/10.1016/j.sandf.2020.09.007.

[61] Lbibb S, Manzari MT. Stress-strain behavior of Ottawa sand in cyclic direct simple shear and modeling of cyclic strength using Artificial Neural Networks. Soil Dynam Earthq Eng 2023;164:107585.

[62] Li N, Yu SM, Wu ER, Song XJ, Jiang P, Xu HB, Wang W. Study on small strain characteristics and microscopic mechanism of rice husk ash modified lime soil. Transport. Geotech. 2024;45:101209. https://doi.org/10.1016/j.trgeo.2024.101209.

[63] Clayton CRI, Priest JA, Bui M, Zervos A, Kim SG. The Stokoe resonant column apparatus: effects of stiffness, mass and specimen fixity. Geotechnique 2009;59:429–37. https://doi.org/10.1680/geot.2007.00096.

[64] Monkul MM, Gültekin C, Gülver M, Akın Ö, Eseller-Bayat E. Estimation of liquefaction potential from dry and saturated sandy soils under drained constant volume cyclic simple shear loading. Soil Dynam Earthq Eng 2015;75:27–36.

[65] Liu S, Qiu Y, Yu W, Zhang H. Highly stretchable and self-healing strain sensor based on gellan gum hybrid hydrogel for human motion monitoring. ACS Appl Polym Mater 2020;2:1325–34.
[66] Jiaer W, Kammerer A, Riemer M, Seed R, Pestana J. Laboratory study of liquefaction triggering criteria. In: 13th world conference on earthquake engineering; 2004. Vancouver, BC, Canada, Paper.
[67] Bouazza A, Gates WP, Ranjith PG. Hydraulic conductivity of biopolymer-treated silty sand. Geotechnique 2009;59:71–2.
[68] Seed HB. Representation of irregular stress time histories by equivalent uniform stress series in liquefaction analyses. National Technical Information Service; 1975.
[69] Cheng K, Zhang Y. A cyclic resistance ratio model of sand-fines mixtures based on cyclic triaxial test. Geotech Geol Eng 2024;42:1021–33. https://doi.org/10.1007/s10706-023-02602-6.
[70] El Takch A, Sadrekarimi A, El Naggar H. Cyclic resistance and liquefaction behavior of silt and sandy silt soils. Soil Dynam Earthq Eng 2016;83:98–109.
[71] Suazo G, Fourie A, Doherty J, Hasan A. Effects of confining stress, density and initial static shear stress on the cyclic shear response of fine-grained unclassified tailings. Geotechnique 2016;66:401–12. https://doi.org/10.1680/jgeot.15.P.032.
[72] Boulanger RW, Idriss IM. Evaluating the potential for liquefaction or cyclic failure of silts and clays. 2004. Citeseer.
[73] Nam-Hong Park J-HK, Jang Yong-Chae, Kim Kwang-Tae, Bae Jeong-Ju, Choi Choong-Rak, Ko Deok-Hyung, Kim Ik-Hyun, Jang Ji-Ho, Song Young-Seok, Kim Cheol-Hwan, Shin Seung-Koo, Oh Se-Beom, Kim Dong-Hyun, Lee Hwa-Soo, Joon-Young Park. Korea design standard 64 17 00. 2018.
[74] Ueng T-S, Chen J-C. Computational procedures for determining parameters in Ramberg-Osgood elastoplastic model based on modulus and damping versus strain. Livermore, CA (United States): Lawrence Livermore National Lab.(LLNL); 1992. https://doi.org/10.2172/6496483.
[75] Ahmad M, Ray R. Comparison between ramberg-osgood and hardin-drnevich soil models in midas GTS NX. Pollack Period 2021;16:52–7. https://doi.org/10.1556/606.2021.00353.
[76] Darendeli MB. Development of a new family of normalized modulus reduction and material damping curves. The university of Texas at Austin; 2001.
[77] Ayeldeen MK, Negm AM, El Sawwaf MA. Evaluating the physical characteristics of biopolymer/soil mixtures. Arabian J Geosci 2016;9:1–13. https://doi.org/10.1007/s12517-016-2366-1.
[78] Anandha Kumar S, Sujatha ER, Pugazhendi A, Jamal MT. Guar gum-stabilized soil: a clean, sustainable and economic alternative liner material for landfills. Clean Technol Environ Policy 2021:1–19. https://doi.org/10.1007/s10098-021-02032-z.
[79] Vucetic M. Cyclic threshold shear strains in soils. J Geotech Eng -Asce 1994;120:2208–28. https://doi.org/10.1061/(Asce)0733-9410(1994)120:12(2208.
[80] Bolton M, Wilson J. Soil stiffness and damping. In: Structural dynamics-vol 1. Routledge; 2022. p. 209–16.
[81] Ellis E, Soga K, Bransby M, Sato M. Resonant column testing of sands with different viscosity pore fluids. J Geotech Geoenviron Eng 2000;126:10–7.
[82] Ta XH, Abbasi B, Muhunthan B, Noh D-H, Kwon T-H. Low-frequency seismic responses during microbial biofilm formation in sands. Environ Geotech 2021;9:524–33.
[83] Im J. Polysaccharide biopolymers in sands: properties and behaviors. In: Department of Civil and environmental engineering, Korea advanced Institute of science and Technology, Korea advanced Institute of science and Technology; 2020.
[84] Chang I, Im J, Cho G-C. Geotechnical engineering behaviors of gellan gum biopolymer treated sand. Can Geotech J 2016;53:1658–70.
[85] Güllü H, Pala M. On the resonance effect by dynamic soil–structure interaction: a revelation study. Nat Hazards 2014;72:827–47.
[86] Xiao P, Liu HL, Xiao Y, Stuedlein AW, Evans TM. Liquefaction resistance of bio-cemented calcareous sand. Soil Dynam Earthq Eng 2018;107:9–19. https://doi.org/10.1016/j.soildyn.2018.01.008.
[87] Porcino D, Marcianò V, Granata R. Cyclic liquefaction behaviour of a moderately cemented grouted sand under repeated loading. Soil Dynam Earthq Eng 2015;79:36–46. https://doi.org/10.1016/j.soildyn.2015.08.006.
[88] Boulanger RW, Idriss I. Closure to "liquefaction susceptibility criteria for silts and clays" by ross W. Boulanger and IM Idriss. J Geotech Geoenviron Eng 2008;134:1027–8. https://doi.org/10.1061/(ASCE)1090-0241(2008)134:7(1027.
[89] Khachatoorian R, Petrisor IG, Kwan CC, Yen TF. Biopolymer plugging effect: laboratory-pressurized pumping flow studies. J Petrol Sci Eng 2003;38:13–21. https://doi.org/10.1016/S0920-4105(03)00019-6.
[90] Lee M, Im J, Chang I, Cho G-C. Evaluation of Injection capabilities of a biopolymer-based grout material. https://doi.org/10.12989/gae.2021.25.1.031; 2021.
[91] Ryou JE, Jung J. Penetration behavior of biopolymer aqueous solutions considering rheological properties. Geomech Eng 2022;29:259–67. https://doi.org/10.12989/gae.2022.29.3.259.